ACS Sustainable Chemistry & Engineering

Letter

pubs.acs.org/journal/ascecg

Low-Temperature Green Synthesis of Multivalent Manganese Oxide Nanowires

Harish Veeramani,[†,∥,*] Deborah Aruguete,[‡] Niven Monsegue,[§] Mitsuhiro Murayama,[§,∥] Urs Dippon,[⊥] Andreas Kappler,[⊥] and Michael F. Hochella[†,∥]

[†]Center for NanoBioEarth, Department of Geosciences, Virginia Tech, Blacksburg, Virginia 24061, United States

[‡]Division of Earth Sciences, National Science Foundation, Arlington, Virginia 22230, United States

[§]Department of Materials Science and Engineering, Virginia Tech, Blacksburg, Virginia 24061, United States

[∥]Institute for Critical Technology and Applied Science, Virginia Tech, Blacksburg, Virginia 24061, United States

[⊥]Geomicrobiology, Center for Applied Geoscience, Eberhard-Karls-University Tuebingen, 72076 Tuebingen, Germany

Supporting Information

ABSTRACT: Manganese oxide nanomaterials hold promise for sustainable nanotechnologies given their utility for a variety of applications, the Earth's abundance of manganese, and their low toxicity relative to other nanomaterials. However green scalable synthesis methods for such nanomaterials are needed. We report here a green room-temperature synthesis of polycrystalline Mn_3O_4 nanowires. In this procedure, aqueous Mn(II) is oxidized under circumneutral conditions by atmospheric oxygen in the presence of nanocrystalline iron oxide (α-Fe_2O_3), an inexpensive catalyst, and a classic biochemical Good's buffer, PIPES (piperazine-N,N^I-bis(2-ethanesulfonic acid). The synthesis method is novel due to its simplicity, minimal energy input and waste output, and potential scalability. The Mn_3O_4 nanowires have been characterized with a suite of electron microscopy techniques.

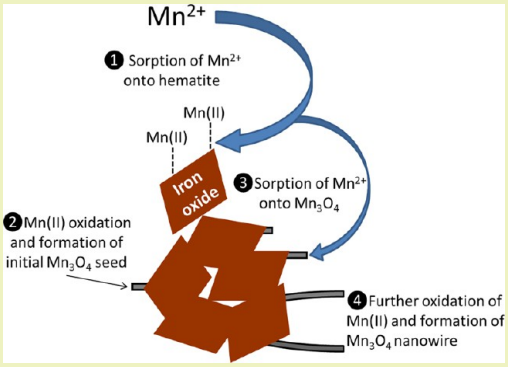

KEYWORDS: *Nanotechnology, Nanowire, Manganese, Oxidation, Prismatic, Iron oxide, Catalyst, Sustainable*

INTRODUCTION

Manganese oxide nanomaterials potentially hold great promise for sustainable nanotechnology. In addition to being of high interest for a variety of applications, they are based upon Earth-abundant elements, as manganese is the twelfth most abundant element on the planet and the third most common transition element after iron and titanium.[1] Indeed, recent examples demonstrate the potential for manganese oxides, including nanomaterials, to replace technologies based upon scarce elements such as platinum catalytic converters for automobile emissions.[2−6] Manganese oxides also are generally lower toxicity compounds than other materials upon which nanomaterials are commonly based, such as various chalcogenides. One of the manganese oxides of interest for multiple technologies and the focus of this study is Mn_3O_4, also known as hausmannite. Mn_3O_4 is a mixed valence oxide that has been a promising candidate for a range of applications including use as catalysts,[7−10] microwave absorption materials,[11] sensors,[12] supercapacitors,[13−15] and anode materials.[16] Mn_3O_4 nanostructures could also potentially be used as precursors for the production of $LiMn_2O_4$, a material used for battery manufacturing.[17]

In addition to using abundant or renewable raw source materials that have low toxicity, a frequently important factor in the development of sustainable nanotechnologies is the ability to produce nanomaterials according to green chemistry principles. We have considered for our investigation Mn_3O_4 nanowires, as nanowires are of particular interest for their application in device technologies. With regards to Mn_3O_4 nanowires, a variety of synthetic methods have been developed that frequently entail hydrothermal techniques, often carried out at high temperature and pressure in the presence of solvents, concentrated acids, bases, and templates.[18−22] A few of the major disadvantages of high-temperature nanowire synthesis methods include their high cost of fabrication and scale-up challenges to produce larger amounts of nanowires.[23] Researchers have begun to examine greener syntheses of Mn_3O_4 nanomaterials, via sol−gel processes[24,25] and ionic liquids,[26,27] but most of these methods still involve post-treatment at higher temperatures.[25,27,28]

As an alternative to such methods, we present in this letter a room-temperature synthesis of Mn_3O_4 nanowires solely from water and manganese salt, catalyzed by iron oxide (α-Fe_2O_3, also known as hematite) nanocrystals in the presence of a classic biochemical buffer, PIPES (piperazine-N,N^I-bis(2-ethanesulfonic acid). We describe our characterization of the

Received: April 29, 2013
Revised: June 17, 2013
Published: June 26, 2013

Mn_3O_4 nanowires with conventional and high-resolution electron microscopy, X-ray diffraction, and electron energy loss spectroscopy and atomic force microscopy.

EXPERIMENTAL SECTION

All chemicals used were of ultrapure analytical grade. Glassware was cleaned by soaking in 10% (v/v) HCl overnight followed by five rinses with deionized water and ultrapure water (18.2 MΩ cm resistivity) prior to use. The iron oxide nanocrystal catalyst was synthesized by forced hydrolysis of an acidic ferric salt solution ($Fe(NO_3)_3{\cdot}9H_2O$, Fisher Scientific, 99.4% pure, ACS grade) according to one of the methods described by Schwertmann and Cornell.[29] Briefly the method involves aging of a ferric nitrate solution at 98 °C for 7 days followed by dialysis to remove residual salts. The iron oxide catalyst was characterized by transmission electron microscopy (TEM) (Figure S1A, Supporting Information), X-ray powder diffraction (XRD) (Figure S1B, Supporting Information), and Mössbauer spectroscopy (Figure S2, Supporting Information) prior to the experiment. Mössbauer spectroscopic measurements at room, liquid nitrogen (77 K), and near liquid He (4.2 K) temperatures were obtained to investigate oxidation and coordination states of Fe environments in the catalyst to determine the purity of the iron oxide phase. Details of the sample preparation for XRD and Mössbauer spectroscopy are included in the Supporting Information. The synthesis was as follows: 20 mg of the iron oxide nanocrystals and 1 mL of (1 M stock) PIPES buffer [piperazine-N,N^I-bis(2-ethanesulfonic acid)] were added to 50 mL ultrapure water (18.2 MΩ cm resistivity). The pH was adjusted to 7.5 by adding a few drops of 0.5 M NaOH or HCl. Under magnetic stirring, the formation of Mn_3O_4 nanowires was initiated by adding an aliquot of aqueous $MnCl_2$ (Sigma-Aldrich; 1 M stock) to the iron oxide nanocrystal suspension to bring the reaction mixture to an initial $Mn(II)_{aq}$ concentration of 0.001 M. The drift in pH was monitored at regular intervals prior to every sampling and adjusted using 0.5 M NaOH when necessary. The synthesis was performed entirely at room temperature under oxic conditions. $Mn(II)_{aq}$ in the reaction mixture was analyzed by the a modified formaldoxime spectrophotometric method similar to that reported elsewhere.[30,31] Details of the Mn(II) analysis, assay conditions, and sample preparation for electron microscopy are elaborated in the Supporting Information.

Scanning electron microscopy (SEM) images were acquired using the LEO-Zeiss 1550 SEM with a Schottky field-emission gun using an accelerating voltage of 5 kilovolts (kV), working distance of 5 mm, and an in-lens detector. All TEM work, including high-resolution TEM (HR-TEM), scanning TEM (STEM)−high angle annular dark field (HAADF) imaging, electron diffraction with nanometer size parallel beam illumination, electron tomography, and energy dispersive X-ray spectroscopy (EDS) was carried out using a FEI TITAN 300 operated at 300 kV. Electron energy loss spectroscopy (EELS) spectra and Fe, Mn, and O elemental maps were recorded by means of a Gatan (Warrendale, PA) imaging filter (GIF-Tridiem 863) controlled by Gatan Digital Micrograph software. X-ray powder diffraction was performed on a Rigaku Miniflex X-ray powder diffractometer using monochromated Cu Kα radiation to identify the manganese oxide phase in the synthesized product. Further details of sample preparation and analysis are provided in the Supporting Information. The Mn_3O_4 nanowires were also imaged using a Veeco multimode atomic force microscope (Veeco Metrology, Santa Barbara, CA) in the tapping mode. Analysis of the AFM images was carried out using the Digital Instruments, NanoScope IIIa software. Details of the sample preparation for AFM measurements and instrument settings are provided in the Supporting Information.

RESULTS AND DISCUSSION

The iron oxide catalyst (Figure S1A, Supporting Information) synthesized by forced hydrolysis of ferric nitrate yielded pure hematite as confirmed by powder X-ray diffraction (Figure S1B, Supporting Information) and Mossbauer analysis (Figure S2, Supporting Information). The absence of other peaks in the X-ray diffractogram is indicative of a pure hematite phase. The derived Mössbauer spectral parameters at all tested temperatures are in agreement with the hematite reference and indicative of a pure phase. The catalytic activity of iron oxide nanoparticles is evident by their propensity to oxidize aqueous Mn(II)[32] under oxic conditions. As shown in Figure 1, Mn(II) oxidation is complete over a course of 48 h in the presence of iron oxide. In the absence of iron oxides, the concentration of $Mn(II)_{aq}$ remains relatively constant indicating the importance of surface catalysis in the formation of Mn_3O_4. The XRD powder diffraction pattern taken from the suspension after complete Mn(II) oxidation confirmed the presence of hausmannite (Mn_3O_4) and hematite (Fe_2O_3) (Figure S3, Supporting Information). HR-TEM images of the reaction mixture after complete Mn(II) oxidation reveals Mn_3O_4 nanowires that are approximately 7 nm in diameter (Figure 2A). This is consistent with AFM measurements that indicate a similar vertical distance (7.2−7.5 nm) for individual or isolated nanowires (Figure S4, Supporting Information). Lattice fringes are observed along the length of the nanowire indicating its crystalline nature. Selected area electron diffraction (SAED) analysis of the sample (data not shown) and fast Fourier transform (FFT) analysis (Figure 2A insert) of the HR-TEM

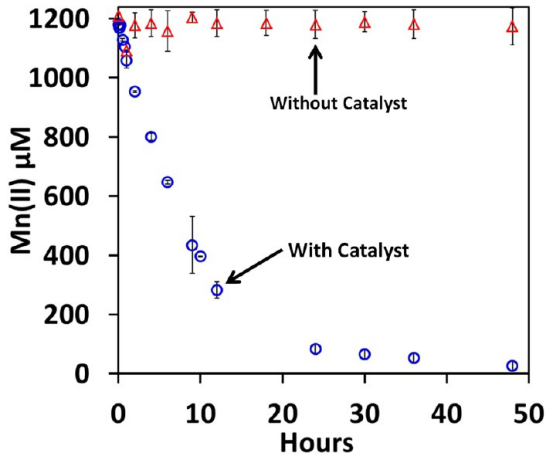

Figure 1. Aqueous Mn(II) oxidation catalyzed by iron oxide (hematite) nanoparticles. Error bars represent the standard deviation between replicate experimental runs.

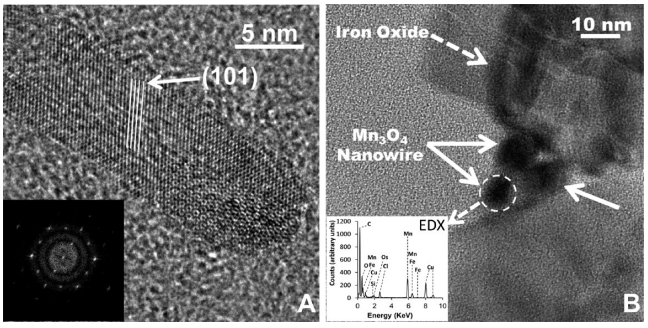

Figure 2. (A) High-resolution TEM image of the Mn_3O_4 nanowire exhibits lattice fringes. Insert shows a FFT pattern of the HRTEM image. (B) TEM image of a thin section of an aggregate shows the prismatic cross section of three nanowires. Insert demonstrates elemental composition (EDS) of one of the nanowires. The Cu and C signals in the EDX are due to the carbon-coated copper grid that was used for TEM analysis and the Os, Cl, and Si signals are due to the resin that was used for ultra microtomy.

dx.doi.org/10.1021/sc400129n | ACS Sustainable Chem. Eng. 2013, 1, 1070−1074

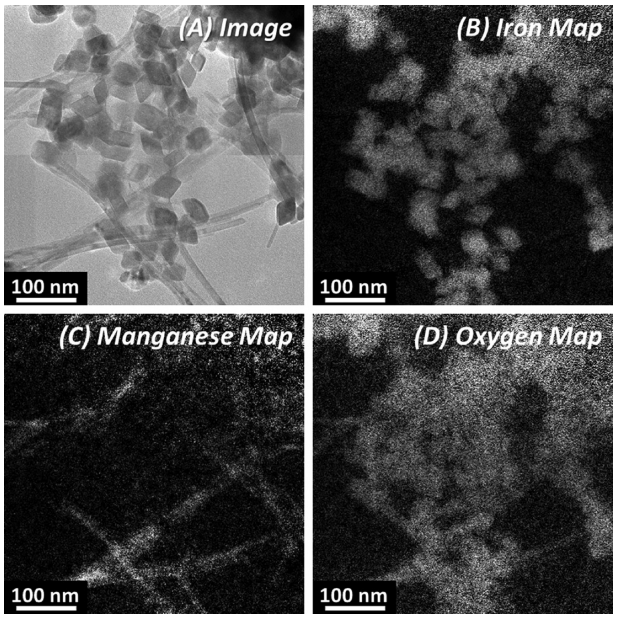

Figure 3. (A) TEM image of rhombohedral iron oxide nanoparticles and MnO_2 nanowires. (B) Iron (Fe $L_{2,3}$ edge) EELS map highlighting the iron oxide nanoparticles. (C) Mn (Mn $L_{2,3}$ edge) EELS map highlighting the Mn_3O_4 nanowires. (D) Oxygen (O K edge) EELS map highlighting both the iron oxide and Mn_3O_4 nanowires.

images indicate the presence of lattice spacings matching those of Mn_3O_4, specifically hausmannite (space group: $I4_1/amd$; lattice constant: a = b = 5.765 Å and c = 9.442 Å). Variations in the FFT pattern along the length of the nanowire suggest a gradual change in the crystallographic orientation relative to the wire's longitudinal axis presumably due to twisting of the wire along its length. Cross sections of the Mn_3O_4 nanowires are seen in the microtomed thin section (Figure 2B). The three nanowires that are seen between two iron oxide particles in the middle of the TEM image exhibit a prismatic geometry. Elemental analysis (EDS) on the cross section of a nanowire (circled) indicated that the nanowires are composed mainly of Mn and O (Figure 2B insert). All three nanowires showed identical chemical composition. EELS mapping of a field containing multiple Mn_3O_4 nanowires highlights Mn and O (Figure 3).

SEM images taken at various times during an experiment demonstrate the growth of Mn_3O_4 nanowires with time (Figure 4). The Mn(II) oxidation product exhibits a transient short rod-like morphology between 4 and 12 h after initiating the reaction. These nanorods grow longer with increasing abundance in 24 h, beyond which the fibers seem to exhibit flexibility, evident from bending of the longer nanowires as shown in the SEM images (Figure 4). As expected from the solution chemistry shown in Figure 1, Mn_3O_4 nanowires were not observed in the control experiments lacking the iron oxide catalyst (Figure S5, Supporting Information).

The iron oxide catalyst used during Mn_3O_4 nanowire synthesis does not undergo any phase transformation (confirmed by Mössbauer spectroscopy, data not shown) suggesting that it could be potentially reused for synthesizing Mn_3O_4 nanowires contingent upon the development of a method to separate the iron oxide catalyst nanoparticles from the reaction mixture. Alternately, the iron oxide (Fe_2O_3) and Mn_3O_4 nanowire mixture could be useful for the mechano-chemical synthesis of manganese ferrite that is used in the electronic industry and as starting material for manufacturing

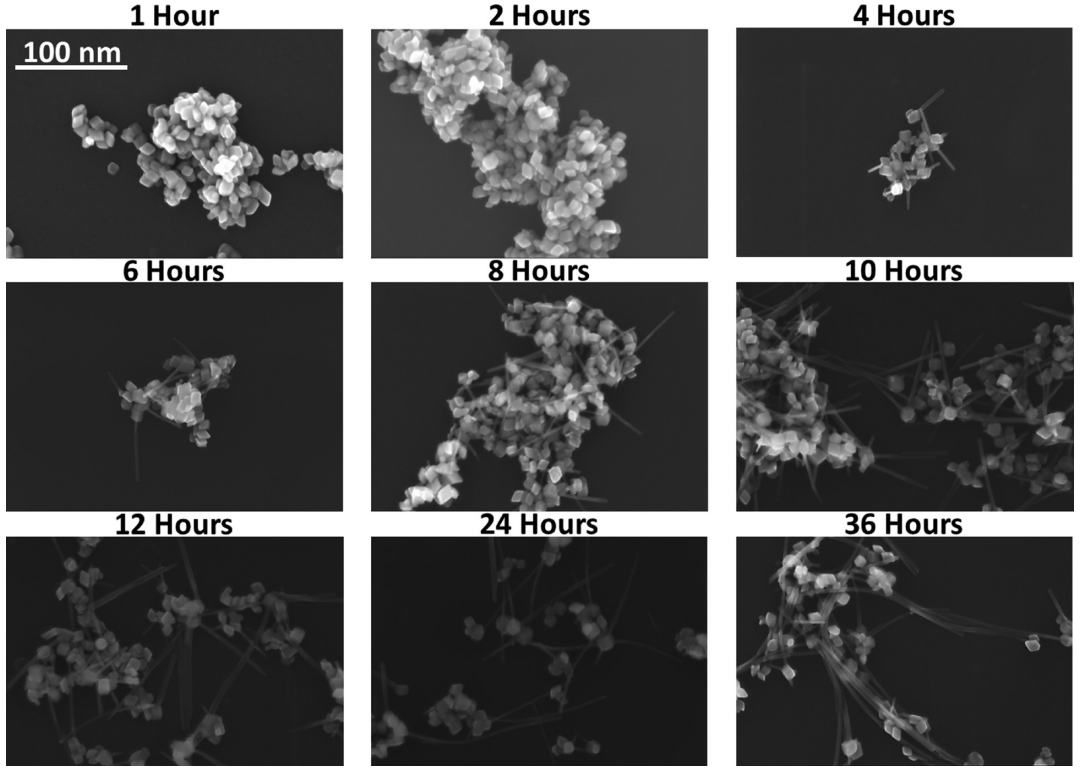

Figure 4. Formation and growth of Mn_3O_4 nanowire as seen by SEM. All images are at the same magnification with the scale bar shown in the top left image panel.

ceramics.[33] The mechanism of heterogeneous Mn(II) oxidation is believed to be composed of several elementary steps. The oxidation of Mn^{2+}_{aq} proceeds fast when surfaces such as iron oxides are available for Mn(II) sorption. The oxygen atoms from dissociated hydroxyl groups on the iron oxide surfaces are capable of donating electron density to adsorbed Mn(II) species thus encouraging the transfer of electrons from Mn(II) to O_2. Consequently, the adsorbed Mn(II) oxidizes to Mn(III), which eventually becomes incorporated into a growing manganese oxide precipitate as the reaction proceeds by the autocatalytic mechanism. The mechanism of Mn(II) oxidation in the presence of iron oxide surfaces has been extensively discussed by Madden and Hochella.[32]

The origin of a nanowire morphology for the Mn_3O_4, which has not been previously observed for Mn oxidation catalyzed by hematite[32] nanocrystals, may potentially lie in the use of PIPES as a buffer. Xie and co-workers reported the formation of branched gold nanoparticles, as opposed to spherical nanoparticles, in the presence of Good's buffers[34] with a piperazine moiety (including PIPES). They also reported the formation of gold nanoflowers in the presence specifically of HEPES (a Good's buffer with similarities to PIPES).[35] It was inferred that differential adsorption of buffer molecules onto different crystal faces could cause the growth of nonspherical structures.[34] Additional prior work exploring the use of buffers in gold nanoparticle synthesis has indicated via voltammetric measurements that buffers, including Good's buffers, can adsorb strongly to gold surfaces.[36] The influence of the PIPES buffer on crystal growth in the present system is unknown, and future work is needed to systematically investigate the effect of PIPES and related buffers on the growth and morphology of the Mn_3O_4 nanowires.

In summary, we have presented a room-temperature synthesis of Mn_3O_4 nanowires, solely using manganese chloride, water, iron oxide nanoparticles as a catalyst, and a buffer (PIPES). The synthesis is conducted in air, with atmospheric oxygen acting as the oxidizer in the reaction. Electron microscopy and diffraction indicate that the nanowires produced are solid (not hollow) and highly crystalline. With a limited number of precursor ingredients, water as the primary solvent, minimal energy input, and minimal waste output, these results suggest an exciting approach in green nanomaterials synthesis to be further explored.

■ ASSOCIATED CONTENT

Ⓢ Supporting Information

Information as mentioned in the text. This material is available free of charge via the Internet at http://pubs.acs.org.

■ AUTHOR INFORMATION

Corresponding Author

*E-mail: harish@vt.edu.

Notes

The authors declare no competing financial interest.

■ ACKNOWLEDGMENTS

Funding for this project was provided by grants from the U.S. Department of Energy (DE-PS02-09ER09-02) and the Institute for Critical Technology and Applied Science (ICTAS) at Virginia Tech. We acknowledge the NCFL (Nanoscale Characterization and Fabrication Laboratory) at ICTAS. We thank Steven McCartney (NCFL), Weinan Leng (ICTAS), and Kathy Lowe (VA-MD Regional College of Veterinary Medicine) for providing assistance with the SEM analysis, AFM measurements, and ultramicrotomy respectively. D.M.A. completed this manuscript during her service at the National Science Foundation (NSF). Views, opinions, and findings described in this manuscript are those of the authors and not necessarily those of NSF.

■ REFERENCES

(1) Earnshaw, A.; Greenwood, N. N. *Chemistry of the Elements*, 2nd ed.; Butterworth-Heinemann: Oxford, U.K., 1997.

(2) Katz, M. The Heterogeneous Oxidation of Carbon Monoxide. In *Advance in Catalysis*; Frankenburg, W. G., Komarewsky, V. I., Eds.; Academic Press: New York, 1953; Vol. 5, pp 177−216.

(3) Zaki, M. I.; Hasan, M. A.; Pasupulety, L.; Kumari, K. Thermochemistry of manganese oxides in reactive gas atmospheres: Probing catalytic MnO_x compositions in the atmosphere of $CO+O_2$. *Thermochim. Acta* **1998**, *311* (1−2), 97−103.

(4) Han, Y.-F.; Chen, F.; Zhong, Z.; Ramesh, K.; Chen, L.; Widjaja, E. Controlled synthesis, characterization, and catalytic properties of Mn_2O_3 and Mn_3O_4 nanoparticles supported on mesoporous silica SBA-15. *J. Phys. Chem. B* **2006**, *110* (48), 24450−24456.

(5) Iablokov, V.; Frey, K.; Geszti, O.; Kruse, N. High catalytic activity in CO oxidation over MnO_x nanocrystals. *Catal. Lett.* **2010**, *134* (3−4), 210−216.

(6) Wang, W.; McCool, G.; Kapur, N.; Yuan, G.; Shan, B.; Nguyen, M.; Graham, U. M.; Davis, B. H.; Jacobs, G.; Cho, K.; Hao, X. Mixed-phase oxide catalyst based on Mn-Mullite (Sm, Gd)Mn_2O_5 for NO oxidation in diesel exhaust. *Science* **2012**, *337* (6096), 832−835.

(7) Moggridge, G. D.; Rayment, T.; Lambert, R. M. An in situ XRD investigation of singly and doubly promoted manganese oxide methane coupling catalysts. *J. Catal.* **1992**, *134* (1), 242−252.

(8) Tian, Z.-R.; Tong, W.; Wang, J.-Y.; Duan, N.-G.; Krishnan, V. V.; Suib, S. L. Manganese oxide mesoporous structures: Mixed-valent semiconducting catalysts. *Science* **1997**, *276* (5314), 926−930.

(9) Zhang, P.; Zhan, Y.; Cai, B.; Hao, C.; Wang, J.; Liu, C.; Meng, Z.; Yin, Z.; Chen, Q. Shape-controlled synthesis of Mn_3O_4 nanocrystals and their catalysis of the degradation of methylene blue. *Nano Res.* **2010**, *3* (4), 235−243.

(10) Zhang, J.; Du, J.; Wang, H.; Wang, J.; Qu, Z.; Jia, L. A novel mild route to hausmannite Mn_3O_4 nanocubes at room temperature and its catalytic performance. *Mater. Lett.* **2011**, *65* (17−18), 2565−2567.

(11) Yan, D.; Cheng, S.; Zhuo, R. F.; Chen, J. T.; Feng, J. J.; Feng, H. T.; Li, H. J.; Wu, Z. G.; Wang, J.; Yan, P. X. Nanoparticles and 3D sponge-like porous networks of manganese oxides and their microwave absorption properties. *Nanotechnology* **2009**, *20* (10), 105706.

(12) Zhang, L.; Zhou, Q.; Liu, Z.; Hou, X.; Li, Y.; Lv, Y. Novel Mn_3O_4 Micro-octahedra: promising cataluminescence sensing material for acetone. *Chem. Mater.* **2009**, *21* (21), 5066−5071.

(13) Dai, Y.; Wang, K.; Xie, J. From spinel Mn_3O_4 to layered nanoarchitectures using electrochemical cycling and the distinctive pseudocapacitive behavior. *Appl. Phys. Lett.* **2007**, *90* (10), 104102.

(14) Hu, C.-C.; Wu, Y.-T.; Chang, K.-H. Low-temperature hydrothermal synthesis of Mn_3O_4 and MnOOH single crystals: Determinant influence of oxidants. *Chem. Mater.* **2008**, *20* (9), 2890−2894.

(15) Jiang, J.; Kucernak, A. Electrochemical supercapacitor material based on manganese oxide: Preparation and characterization. *Electrochim. Acta* **2002**, *47* (15), 2381−2386.

(16) Wang, H.; Cui, L.-F.; Yang, Y.; Sanchez Casalongue, H.; Robinson, J. T.; Liang, Y.; Cui, Y.; Dai, H. Mn_3O_4−Graphene hybrid as a high-capacity anode material for lithium ion batteries. *J. Am. Chem. Soc.* **2010**, *132* (40), 13978−13980.

(17) Zhang, X.; Xing, Z.; Yu, Y.; Li, Q.; Tang, K.; Huang, T.; Zhu, Y.; Qian, Y.; Chen, D. Synthesis of Mn_3O_4 nanowires and their transformation to $LiMn_2O_4$ polyhedrons, application of $LiMn_2O_4$ as

a cathode in a lithium-ion battery. *CrystEngComm* **2012**, *14* (4), 1485−1489.
(18) Wang, X.; Li, Y. Selected-control hydrothermal synthesis of α- and β-MnO_2 single crystal nanowires. *J. Am. Chem. Soc.* **2002**, *124* (12), 2880−2881.
(19) Wang, X.; Li, Y. Synthesis and formation mechanism of manganese dioxide nanowires/nanorods. *Chem.—Eur. J.* **2003**, *9* (1), 300−306.
(20) Zhang, G.-Q.; Bao, S.-J.; Zhang, X.-G.; Li, H.-L. Influence of cation (NH^{4+}) on electrochemical characteristics of MnO_2 nanowire synthesized by hydrothermal method. *J. Solid State Electrochem.* **2005**, *9* (10), 655−659.
(21) Wang, X.; Wang, X.; Huang, W.; Sebastian, P. J.; Gamboa, S. Sol−gel template synthesis of highly ordered MnO_2 nanowire arrays. *J. Power Sources* **2005**, *140* (1), 211−215.
(22) Wang, H.-q.; Zheng, M.-b.; Chen, J.-h.; Ji, G.-b.; Cao, J.-m., Synthesis of MnO_2 microfiber with secondary nanostructure by cotton template. *J. Nanotechnol.* **2012**, *2010*.
(23) Law, M.; Goldberger, J.; Yang, P. Semiconductor nanowires and nanotubes. *Annu. Rev. Mater. Res.* **2004**, *34* (1), 83−122.
(24) Vázquez-Olmos, A.; Redón, R.; Rodríguez-Gattorno, G.; Esther Mata-Zamora, M.; Morales-Leal, F.; Fernández-Osorio, A. L.; Saniger, J. M. One-step synthesis of Mn_3O_4 nanoparticles: Structural and magnetic study. *J. Colloid Interface Sci.* **2005**, *291* (1), 175−180.
(25) Seo, W. S.; Jo, H. H.; Lee, K.; Kim, B.; Oh, S. J.; Park, J. T. Size-dependent magnetic properties of colloidal Mn_3O_4 and MnO nanoparticles. *Angew. Chem., Int. Ed.* **2004**, *43* (9), 1115−1117.
(26) Durmus, Z.; Kavas, H.; Baykal, A.; Toprak, M. A green chemical route for the synthesis of Mn_3O_4 nanoparticles. *Cent. Eur. J. Chem.* **2009**, *7* (3), 555−559.
(27) Gunay, M.; Baykal, A.; Toprak, M.; Sozeri, H. A green chemical synthesis and characterization of Mn_3O_4 nanoparticles. *J. Supercond. Novel Magn.* **2012**, *25* (5), 1535−1539.
(28) Zhang, X.; Yu, P.; Zhang, D.; Zhang, H.; Sun, X.; Ma, Y. Room temperature synthesis of Mn_3O_4 nanoparticles: characterization, electrochemical properties and hydrothermal transformation to γ-MnO_2 nanorods. *Mater. Lett.* **2013**, *92* (0), 401−404.
(29) Schwertmann, U.CornellR. M. *Iron Oxides in the Laboratory: Preparation and Characterization*; Wiley−VCH, Weinheim, Germany, 2000.
(30) Morgan, J. J.; Stumm, W. Analytical chemistry of aqueous manganese. *J. Am. Water Works Assn.* **1965**, *57* (1), 107−119.
(31) Brewer, P. G.; Spencer, D. W. Colorimetric determination of manganese in anoxic waters. *Limnol. Oceanogr.* **1971**, *16* (1), 107−110.
(32) Madden, A.; Hochella, M. A test of geochemical reactivity as a function of mineral size: Manganese oxidation promoted by hematite nanoparticles. *Geochim. Cosmochim. Acta* **2005**, *69* (2), 389−398.
(33) Berbenni, V.; Marini, A.; Profumo, A.; Cucca, L. The effect of high energy milling on the solid state synthesis of $MnFe_2O_4$ from mixtures of MnO−Fe_2O_3 and Mn_3O_4−Fe_2O_3. *Z. Naturforsch. B* **2003**, *58* (5), 415−422.
(34) Xie, J.; Lee, J. Y.; Wang, D. I. C. Seedless, surfactantless, high-yield synthesis of branched gold nanocrystals in HEPES buffer solution. *Chem. Mater.* **2007**, *19* (11), 2823−2830.
(35) Xie, J.; Zhang, Q.; Lee, J. Y.; Wang, D. I. C. The synthesis of SERS-active gold nanoflower tags for in vivo applications. *ACS Nano* **2008**, *2* (12), 2473−2480.
(36) Engelbrekt, C.; Sorensen, K. H.; Zhang, J.; Welinder, A. C.; Jensen, P. S.; Ulstrup, J. Green synthesis of gold nanoparticles with starch-glucose and application in bioelectrochemistry. *J. Mater. Chem.* **2009**, *19* (42), 7839−7847.